Available online at www.sciencedirect.com
ScienceDirect
Journal of Nuclear Materials 374 (2008) 116–122
journal of nuclear materials
www.elsevier.com/locate/jnucmat

Preparation and characterization of ferric oxyhydroxide and ferric oxide thin films by direct-hydrolysis deposition

Dong Fu, J. Clara Wren *

Department of Chemistry, The University of Western Ontario, 1151 Richmond Street, London, Ontario, Canada N6A 5B7

Received 28 December 2006; accepted 16 July 2007

Abstract

We explore a novel wet-chemical process to form ferric oxyhydroxide and oxide films, direct-hydrolysis deposition, in which the substrate is immersed directly into a treatment solution to form films. The preferential film is obtained at a concentration of 20 mmol dm^{-3} $Fe(NO_3)_3$ solution and a reaction temperature of 60 °C. The film can be thickened by re-immersing it into a fresh treatment solution of the same concentration under the same condition, which results in the film thickness in the range of several hundred nm to several μm. Film characterization by Raman, SEM and XRD shows that the initial film is formed as γ-FeOOH. Heating the film in air at 400 °C converts it to α-Fe_2O_3. No other ions are introduced into the film.
© 2007 Elsevier B.V. All rights reserved.

PACS: 81.15.Lm; 28.41.Qb; 81.05.Je; 60

1. Introduction

The heat transport system (HTS) of a CANDU© reactor consists of 2.5 wt% Nb alloy pressure tubes inside the reactor core, connected to carbon steel pipes outside the core. Corrosion of these pipes under reactor operating conditions is a main concern for aging CANDU reactors. Steel corrosion releases metal ions into the coolant, which can precipitate along the circuit, potentially affecting the heat transfer efficiency of the system. Their neutron activation prior to precipitation can increase radioactivity levels outside the reactor core, and pose a safety problem during reactor shutdown and maintenance. Various measures have been taken to minimize these effects, such as coolant purification and filtration and the adoption of pH control to minimize solubility. Concern about steel corrosion is not limited to CANDU, but also to PWR (pressurized water reactor) and BWR (boiling water reactors), although these reactors use stainless steel.

The corrosion of steels is strongly affected by the presence of oxide films, which vary considerably in reactivity and solubility. Generally, corrosion studies have been limited to the low corrosion potential range where carbon steel in de-aerated water is typically poised. In this potential range, the surface oxide film is considered to be mainly magnetite, Fe_3O_4 [1], but more recent studies on the synergistic interaction of water radiolysis and carbon steel corrosion [2] suggest that H_2O_2, produced by radiolysis, can increase the corrosion potential to a range where Fe^{III} oxides, such as Fe_2O_3 and FeOOH, may also form in addition to Fe_3O_4. These surface oxides may interact with water radiolysis products very differently, making it difficult to predict the effect of radiation on steel corrosion, since H_2O_2 may disproportionate on the oxide-covered surfaces ($H_2O_2 \rightarrow \frac{1}{2}O_2 + H_2O$), as well as drive steel corrosion.

Our primary goal is to determine how radiolytic oxidants, such as H_2O_2, will interact with oxide-covered steel surfaces and what influence this will have in steel corrosion kinetics. However, oxide films formed on carbon steel are

* Corresponding author. Tel.: +1 519 661 2111x86339; fax: +1 519 661 3022.
E-mail address: jcwren@uwo.ca (J.C. Wren).

0022-3115/$ - see front matter © 2007 Elsevier B.V. All rights reserved.
doi:10.1016/j.jnucmat.2007.07.014

complex mixtures of several different iron oxides and oxyhydroxides, making the corrosion chemistry of steel notoriously complex. For example, lepidocrocite, γ-FeOOH, is a ubiquitous ferric oxyhydroxide that may enhance the rate of corrosion since it is suspected to act as an electron acceptor towards iron metal [3]. Consequently, we are preparing single-phase oxide films on conducting glasses to facilitate electrochemical and in situ spectroscopy/microscopy measurements on these oxides. By studying the behaviour of H_2O_2 on individual oxides/hydroxides we hope to be able to characterize the more complicated behaviour of carbon steel surfaces in the presence of radiolytically-decomposed water. Here, as a first step in this process, we describe a method to produce a well characterized γ-FeOOH and α-Fe_2O_3 layers.

In general, the thin film preparation techniques can be roughly divided into physical and chemical methods. The physical methods, such as vacuum evaporation and sputtering, lack flexibility and cost effectiveness, but generate thin films with a high degree of control and purity. Chemical methods such as chemical-vapour deposition, spin coating, deep coating, and spray pyrolysis, are more flexible and economic. Some chemical methods also require special equipment such as vacuum chambers and/or spray guns while other chemical methods, such as wet-chemical processes, are economic and require less sophisticated application technology. Wet-chemical processes include: chemical bath deposition (CBD), successive ionic-layer absorption and reaction (SILAR), liquid-phase deposition (LPD) and electroless deposition (ED). These techniques, summarized in several reviews [4–9], have been used to form thin ceramic films at low temperatures (25–100 °C) from aqueous solutions.

For CBD, a complexing agent, such as NH_3 and urea, is used to control pH, and plays the role of a ligand which slows the rate of solid formation and thus promotes film formation over precipitation. The association/dissociation equilibria of the solvated metal complex are replaced by a process in which the ligand of the complex is displaced by a hydroxyl group to form a solid hydroxide compound, and then oxide from the deprotonation of the hydroxide compound. One disadvantage of CBD is that optimization of the complexing agent and pH is difficult and time-consuming.

The distinguishing characteristic of SILAR is the use of alternating aqueous solutions, in which the substrate is first immersed into a metal-salt solution, and then into a hydrolyzing solution. One deposition cycle yields a film several nm thick for metal oxides on substrates. In principle, ion-by-ion growth of the compound film can be achieved via sequential addition of individual atomic layers [4]. For forming a single-phase oxide film, SILAR is time-consuming and/or requires automation of the process.

The LPD technique is based on the overall equilibrium reaction

$$H_{(n-p)}MF_n + p/2H_2O \Longleftrightarrow MO_{p/2} + nHF \quad (1)$$

where p is the charge of the metal cation. The equilibrium will be shifted towards oxide formation, if the hydrogen fluoride concentration is decreased via addition of a fluorine scavenger, such as boric acid [10] or aluminum metal [11]:

$$H_3BO_3 + 4HF \Longleftrightarrow BF_4^- + H_3O^+ + 2H_2O \quad (2)$$

$$Al + 6HF \Longleftrightarrow H_3AlF_6 + 1.5H_2 \quad (3)$$

The LPD technique, however, often leaves the film doped with unwanted ions. For example, a F/Fe atomic ratio of *ca.* 15% was observed in as-deposited films of iron oxyhydroxides prepared by this method. Even when the films were heated at 600 °C for 1 h, the ratio was still 0.19% and a 'pure' iron oxide film could not be obtained [12].

For ED, if a suitable oxidizing agent is present in the solution, a solid oxide film could be formed by an electrochemical reaction in a liquid electrolytic solution but without the application of electrical current [13,14]. The electrochemical reaction employed in ED generally involves oxidation of the dissolved metal ions at room temperature: $Pb(II)_{aq}$ to Pb(IV) oxide [13]; $Tl(I)_{aq}$ to Tl(III) oxide; and $Mn(II)_{aq}$ to Mn(IV) oxide [14]. In this method, an oxidizing agent must be added to the solution, and in some cases, a catalyst is also necessary [15]. All of these wet-chemical methods to form metal-oxide films require a complexing agent, control of pH, and are often time-consuming.

It has been shown that some high oxidation state transition metal cations readily hydrolyze. Monodispersed colloidal particles of transition metal oxides have been also produced via forced hydrolysis by increasing temperatures in aqueous solutions containing single metal cations [16]. In our present study, this direct-hydrolysis concept has been exploited to form iron oxide films on glass. This novel wet-chemical technique, referred to as direct-hydrolysis deposition (DHD), produces iron oxyhydroxide and oxide films with high degrees of purity and uniformity without using any other complexing agent and pH control.

2. Experimental

2.1. Preparation of solutions and substrates

Solutions were prepared with water purified using a NANOpure Diamond UV ultrapure water system from Barnstead International to remove organic and inorganic impurities. Prepared in this manner, the water had a resistivity of 18.2 MΩ cm.

$Fe(NO_3)_3$ (CP, Caledon Laboratories Ltd.) was dissolved at a concentration of 0.7 mol/dm^3 to make the parent solution. The parent solution was diluted to various concentrations for use as treatment solutions for deposition. The solution concentrations used for the film growth ranged from 1 to 100 mmol dm^{-3}.

Glass microscope slides, approximately 1 mm in thickness (Technologist Choice, Bio Nuclear Diagnostics), were

used as substrates. The substrates were cleaned with manual washing powders, followed by ultrasonic cleaning in distilled water for 30 min.

2.2. Direct-hydrolysis deposition process of films

The substrates were immersed in the treatment solutions and suspended vertically. The film deposition time in the oven was 24–48 h and the oven temperature ranged from 30 to 70 °C. The substrates were then removed from the solutions, rinsed with distilled water, and suspended in air to dry at ambient temperature for 24 h. Heat-treatments of the deposited films were carried out in an air flow for 2 h at temperatures ranging from 100 to 600 °C.

2.3. Characterization of the deposited films

The films formed were characterized using X-ray diffraction (XRD), Raman spectroscopy and scanning electron microscopy (SEM). The X-ray diffraction analysis of the deposited films was carried out on a Rigaku RTP 300RC diffractometer (rate 10°/min, step 0.02°) using Co-Kα radiation (45 kV, 160 mA, X-ray wavelength 1.790210 Å). The Raman spectrum of the samples was measured using a Renishaw Ramascope Model 2000 (633 nm laser wavelength, approx. 2 mW at the sample at 100% power, scan from 2000 to 120 cm^{-1}). The surface morphology of the samples was determined using a Hitachi S-4500 scanning electron microscope.

3. Results and discussion

3.1. γ-FeOOH film formation

3.1.1. Optimum conditions for film formation

Iron oxyhydroxide film formation was studied in the $Fe(NO)_3$ concentration range 2–24 mmol dm^{-3} and in the temperature range of 30–70 °C. Deposition was carried out over 24 and 48 h. The pH of the solutions was not controlled and was in the range of 1.5–2.5 prior to film deposition.

Whether a film on the glass substrate was formed or not was easily discerned due to the visible transparent yellow color of the film. Fig. 1 shows the concentration and temperature ranges where the film formation was observed. There was a minimum temperature, 40 °C, below which no film was formed, irrespective of the $Fe(NO)_3$ concentration. For a given temperature, there was a maximum concentration above which no film was formed. This maximum $Fe(NO)_3$ concentration increased with temperature for temperatures below 60 °C, from 8.0 mmol dm^{-3} at 40 °C to 20.0 mmol dm^{-3} at 60 °C. However, the maximum concentration decreased with temperature for temperatures above 60 °C.

As the solution concentration increased, the colour of the film changed from light yellow to orange, indicating a thicker film was formed at higher concentrations. For a given solution concentration, the colour did not change with temperature, or with deposition time (24 vs. 48 h). The SEM micrograph of the cross-section of the film formed at a concentration of 20 mmol dm^{-3} and 60 °C shows the thickness of the film to be *ca.* 100 nm, Fig. 2. The film formed at 8 mmol dm^{-3} and 60 °C, was too thin to be observed with SEM. The SEM micrographs (Fig. 3) show that the films formed at 60 °C are featureless, but with petal-shaped crystallites, 100–200 nm in size, on top. These films were identified as γ-FeOOH by Raman and XRD, discussed in detail below.

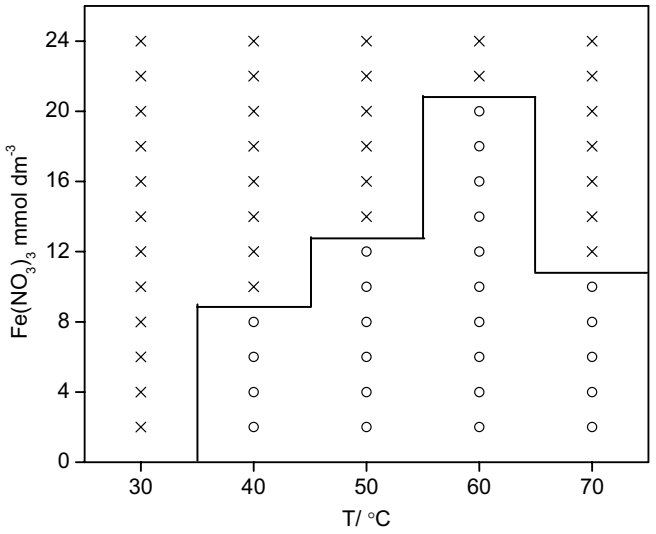

Fig. 1. $Fe(NO_3)_3$ concentration and temperature relationship for forming films. ○ – films formed; × – no film formed.

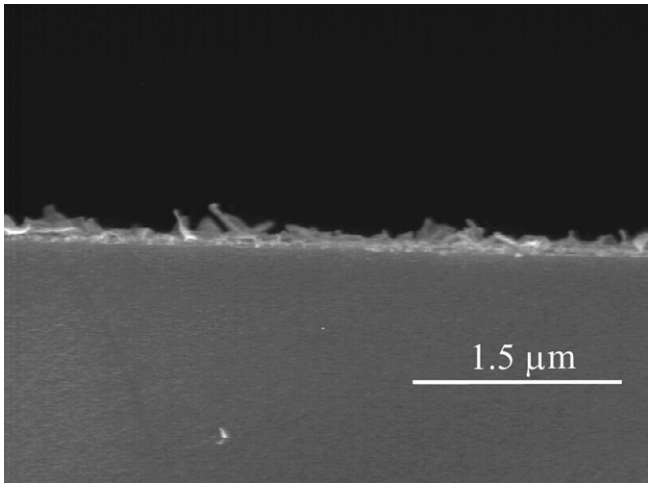

Fig. 2. SEM image of the cross-section of the film formed in an aqueous solution containing 20 mmol dm^{-3} $Fe(NO_3)_3$ at 60 °C.

3.1.2. Film growth on the second deposition cycle

A thicker film was obtained by re-immersing the substrate with the film, formed during the first deposition

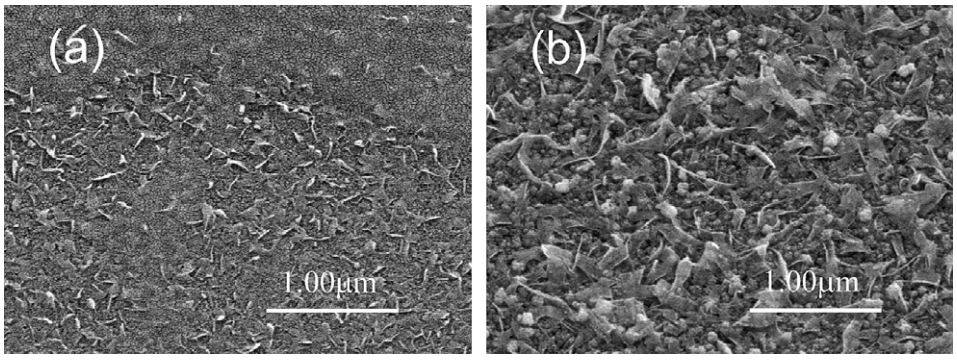

Fig. 3. SEM micrographs of the films formed at 60 °C in aqueous solutions containing: (a) 8 mmol dm^{-3} $Fe(NO_3)_3$; (b) 20 mmol dm^{-3} $Fe(NO_3)_3$.

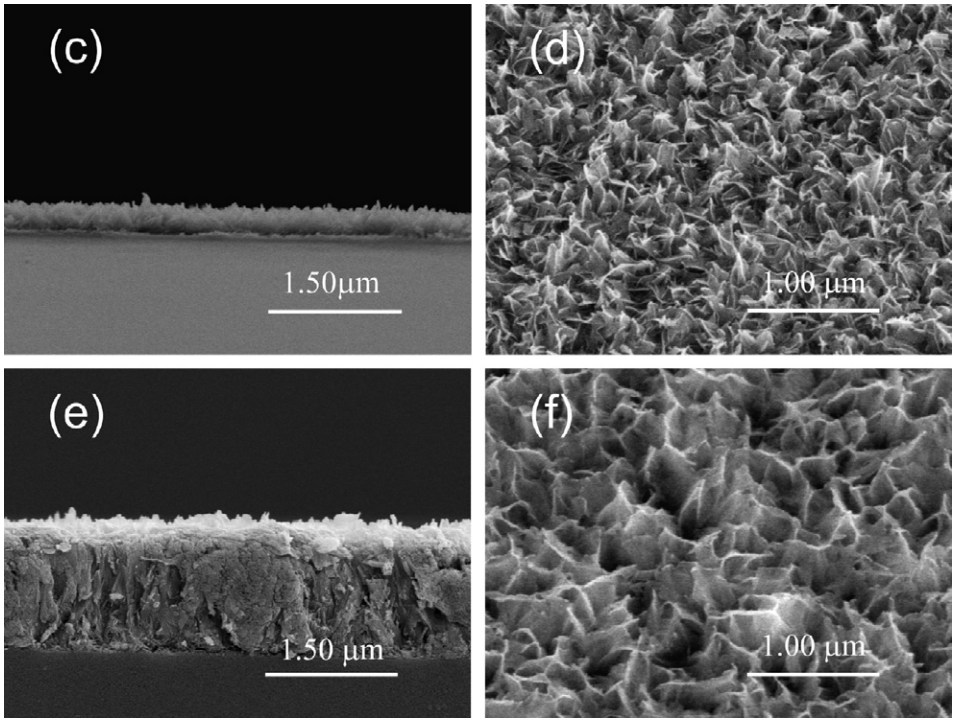

Fig. 4. SEM micrographs of the cross-sections (c) and (e) and surfaces (d) and (f) of the films formed after a second deposition cycle at 60 °C; (c) and (d) in 8 mmol dm^{-3} $Fe(NO_3)_3$ solution, and (e) and (f) in 20 mmol dm^{-3} $Fe(NO_3)_3$ solution.

cycle, into a fresh solution of the same $Fe(NO_3)_3$ concentration at the same reaction temperature for another 24 h. Fig. 4 shows the SEM of the cross-section and surface of the films after the second deposition cycle. For the film formed at 8 mmol dm^{-3} and 60 °C, its thickness increased to *ca.* 300 nm after the second deposition cycle from a film too thin to be observed by SEM after the first cycle. For the film formed at 20 mmol dm^{-3} and 60 °C, its thickness increased from *ca.* 100 nm after the first cycle to *ca.* 1.5 μm after the second cycle. This indicates that the iron oxyhydroxide film grows more easily on a pre-formed film than on clean glass. The surface morphologies of the films formed on the second cycle at 60 °C with the two different concentrations, 8 and 20 mmol dm^{-3} are similar. The petal-shape crystallites grew higher upon the second deposition cycle.

3.1.3. Film characterization

Fig. 5 shows the Raman spectrum of the film formed after the second deposition cycle at 60 °C. All the Raman scattering peaks match with those of γ-FeOOH [17], except two small peaks at 307 and 711 cm^{-1}. The minor peaks are preliminarily assigned: the peak at 307 cm^{-1} to α-FeOOH or γ-Fe_2O_3, and the peak at 711 cm^{-1} to β-FeOOH [17]. These two peaks are, however, very weak, and the main component of the film was γ-FeOOH. The XRD of the film also showed three wide small peaks that match those from γ-FeOOH 200, 301, 321 planes. (The XRD patterns of various films are discussed in details in Section 3.2.)

3.1.4. Proposed film formation mechanism

The pH of the $Fe(NO_3)_3$ solutions prior to film deposition was in the range 1.5–2.5. Ferric ion, Fe^{III}, is octahe-

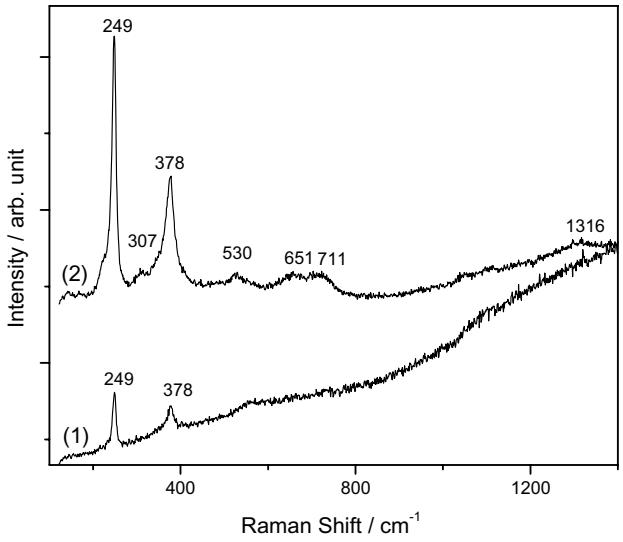

Fig. 5. Raman spectra of the films formed after a second deposition cycle at 60 °C; (1) in 8 mmol dm^{-3} $Fe(NO_3)_3$ solution (2) in 20 mmol dm^{-3} $Fe(NO_3)_3$ solution. Raman spectra were obtained with a laser power at 25% of the full power. Wavenumbers (cm^{-1}) of Raman-active vibrational modes of γ-FeOOH are 255, 380, 528, 654, 1307.

drally coordinated by O^{2-}, OH^-, and H_2O in iron oxide and iron oxyhydroxide formed in acidic environments [18]. In aqueous solutions, Fe^{3+} ion is also octahedrally coordinated and exists as $[Fe(H_2O)_6]^{3+}$ and its acid and base complexes, (i.e., $(Fe(H_2O)_6)^{3+}$) are deprotronated in a stepwise manner to the sequence of species $(Fe(H_2O)_5(OH))^{2+}$, $(Fe(H_2O)_4(OH)_2)^{+}$, ...:

$$(Fe(H_2O)_6)^{3+}(aq) \Longleftrightarrow (Fe(H_2O)_{6-n}(OH)_n)^{3-n}(aq) + nH^+ \quad (4)$$

At a pH of ~ 2 and 70 °C, approximately 70% of iron is present as $(Fe(H_2O)_5(OH)])^{2+}$, 15% as $(Fe(H_2O)_6)^{3+}$, 10% as $(Fe(H_2O)_4(OH)_2)^{+}$, and $(Fe(H_2O)_3(OH)_3)$, $FeNO_3^{2+}$ and $Fe_2(OH)_2^{4+}$ in minor amounts [19].

These Fe^{III} species are deposited and dehydrated on the surface of substrates to form oxyhydroxides, for example:

$$(Fe(H_2O)_3(OH)_3)(aq) \Longleftrightarrow (Fe(H_2O)_3(OH)_3)(\text{on substrates}) \quad (5)$$

$$(Fe(H_2O)_3(OH)_3)(\text{on substrates}) \rightarrow FeOOH(\text{on substrates}) + 5H_2O \quad (6)$$

More hydrated species, $(Fe(H_2O)_4(OH)_2)^{+}$, could deposit on the surface of the substrate and undergo deprotonation and dehydration on the surface.

Dehydration to form FeOOH also occurs in the aqueous phase, resulting in homogeneous precipitation, for example:

$$(Fe(H_2O)_3(OH)_3)(aq) \rightarrow FeOOH(\text{precipitation}) + 5H_2O \quad (7)$$

The rates of the dehydration reactions (6) and (7) increase with temperature, further promoting the formation of more-deprotonated species by shifting the equilibrium reaction (4) to the right [19]. However, as the temperature increases, the equilibrium reaction (5) shifts to the left. This results in a temperature dependence for the rate of the FeOOH formation on surface with a maximum at 60 °C.

The dependence of the film formation on the $Fe(NO_3)_3$ concentration can also be explained by a competition between the homogeneous precipitation and the film formation on surface. Homogeneous precipitation occurs more readily at a higher $Fe(NO_3)_3$ concentration, whereas the film deposition rate, at least initially, depends more on the availability of nucleation sites on the substrate surface. This also explains the extensive growth of the film during the second cycle. At the end of the first deposition cycle, the ferric ion concentration is depleted as a result of the precipitation and the deposition on the substrates and vessel walls. The second deposition cycle using a fresh solution increases the crystal growth considerably, because the ferric ions are replenished in the solution, but also the preformed FeOOH provides nucleation sites for easy crystal growth favouring the dehydration reaction over the precipitation or the deposition on the clean reaction vessel walls.

3.2. α-Fe_2O_3 film formation

3.2.1. Conversion of γ-FeOOH to α-Fe_2O_3

The γ-FeOOH film formed after the second deposition cycle at 20 mmol dm^{-3} and 60 °C was heated at various temperatures, ranging from 100 to 600 °C, for 2 h to dehydrate the oxyhydroxide film to form an oxide film. The film changed colour from orange to dark red upon heating and the red colour was more intense with an increase in the heating temperature.

3.2.2. Film characterization

The Raman spectra of the films heated at various temperatures are shown in Fig. 6. The main component of the film heated at 100 and 200 °C remained γ-FeOOH. However, for the film heated at 300 °C, the Raman intensities of the γ-FeOOH peaks were reduced significantly and several new peaks appeared. At heating temperatures greater than 400 °C, the γ-FeOOH peaks were no longer observed, and only the α-Fe_2O_3 peaks were observed [17], indicating the conversion of the film to α-Fe_2O_3 had been completed.

The XRD patterns of the heat-treated films are consistent with the analysis by Raman spectroscopy (Fig. 7). The three small broad peaks observed for the film treated at 100 °C match γ-FeOOH 200, 301, 321 planes. The broad peaks are indicative of a small crystallite size. Slow hydrolysis of an acidic Fe^{3+} salt forms γ-FeOOH with low crystallinity [20]. The γ-FeOOH film formed by the DHD method is featureless or microcrystalline. Heating of the film at a temperature less than 100 °C does not appear to alter the film. Heated at 300 °C, the γ-FeOOH peaks disappeared, and a weak broad peak at a diffraction angle of 42°, corresponding to the α-Fe_2O_3 1 1 0 plane, appeared, indi-

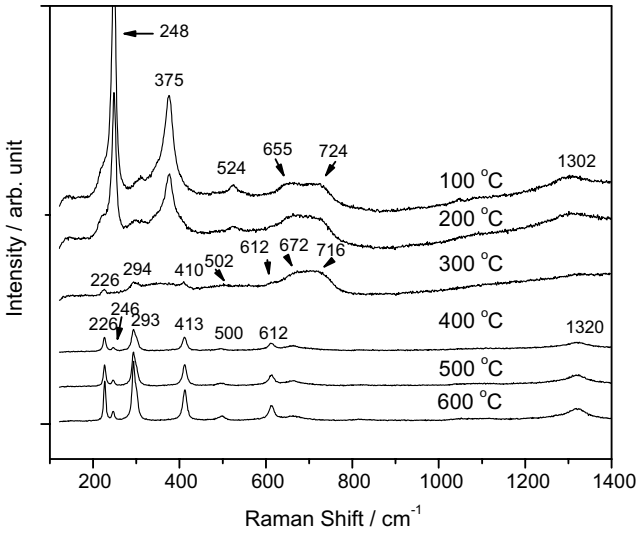

Fig. 6. Raman spectra for the films after heat-treatment at various temperature for 2 h. The films were initially prepared using two deposition cycles in 20 mmol dm^{-3} $Fe(NO_3)_3$ solution at 60 °C and Raman spectrum obtained with a laser power at 25% of the full power. Wavenumbers (cm^{-1}) of Raman-active vibrational modes of γ-FeOOH, 255, 380, 528, 654, 1307; α-Fe_2O_3, 225, 245, 295, 415, 500, 615, 1320.

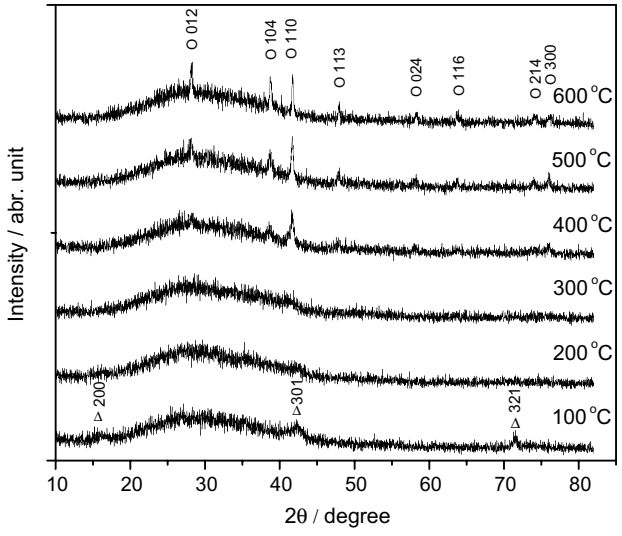

Fig. 7. XRD patterns of the films after heat-treatment at various temperature for 2 h. The films were initially prepared using two deposition cycles in 20 mmol dm^{-3} $Fe(NO_3)_3$ solution at 60 °C. The XRD scattering angles for γ-FeOOH are indicated with symbol Δ and for α-Fe_2O_3 with O.

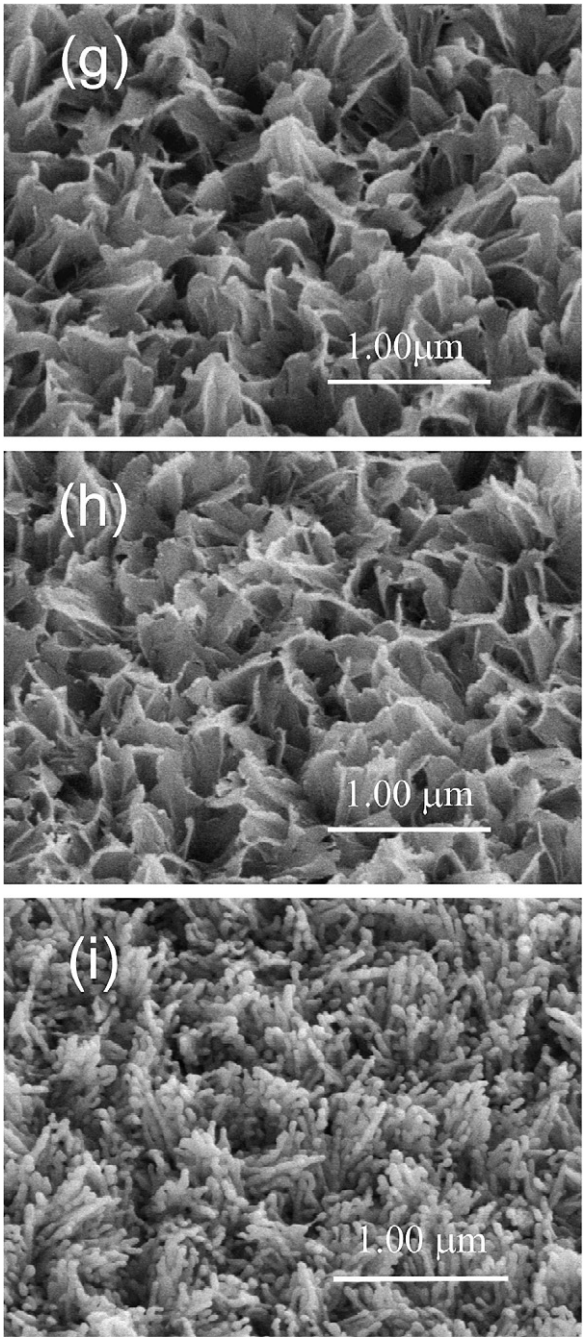

Fig. 8. SEM of the films after heat-treatment at various temperature for 2 h. The films were initially prepared using two deposition cycles in 20 mmol dm^{-3} $Fe(NO_3)_3$ solution at 60 °C. (g) At 200 °C, (h) at 400 °C and (i) at 600 °C.

cating the α-Fe_2O_3 crystal started to form at the expense of the γ-FeOOH crystal. The intensity of the diffraction peak at 42° increased with an increase in the heating temperature (>400 °C). Additional XRD peaks, corresponding to other α-Fe_2O_3 crystal planes, were also observed at higher heating temperatures, indicating that the conversion of γ-FeOOH to the α-Fe_2O_3 crystal increases with heating temperature for temperatures greater than 400 °C.

The SEM images of the heat-treated films show no morphological changes when heated at temperatures below 400 °C, Fig. 8. Only when heated at 600 °C does the morphology of the film change from petal-like to pearl-like crystallites. This observable difference may imply that a larger α-Fe_2O_3 crystal is formed at a high temperature.

With the exception of Fe^{3+} and NO_3^-, no other ions are introduced into the treatment solutions. The films formed are 'pure' ferric oxyhydroxide and oxide films and no ions are introduced in the films.

4. Conclusions

A novel direct-hydrolysis method has been developed for the preparation of pure featureless iron oxyhydroxide and oxide thin films. Conditions have been established that allow control of the thickness of the films over the range 100 nm to 1.5 μm. Heat-treatment of the initially created γ-FeOOH film results in its conversion to α-Fe_2O_3. The extent of the conversion can be controlled by the heat-treatment conditions. At temperatures >400 °C the γ-FeOOH film is completely converted to α-Fe_2O_3. No change in the film morphology is observed with heat-treatment at temperature less than 400 °C. At 600 °C, the morphology of film changes from a petal-like to a pearl-like structure.

We have applied the methods to successfully grow γ-FeOOH and α-Fe_2O_3 on conducting glasses, and the electrochemical properties, and the decomposition kinetics of H_2O_2 of these oxides are being investigated using novel combinations of electrochemical and spectroscopic techniques, such as scanning electrochemical microscopy and confocal Raman microscopy. This new technique for growing specific iron oxyhydroxide films will be used in planned experiments to characterize the corrosion of carbon steel surfaces in the presence of high-energy radiation under controlled conditions. The use of highly specific films will permit the measurement of individual rate constants for reactions with corrosion intermediates that will assist in the establishment of an overall corrosion mechanism under water radiolysis conditions.

Acknowledgements

This work was performed under the Industrial Research Chair Program on Radiation Induced Processes in Nuclear Reactor Environments, funded by Canadian Natural Science and Engineering Research Council (NSERC) and Atomic Energy Canada Ltd. (AECL). The authors wish to thank Ms Heather Bloomfield and Ms Mary Jane Walzak at Surface Science Western for performing SEM and Raman measurements and Kim Law and Jessica Zoe Metcalfe at Department of Earth Science for the X-ray diffraction measurements. The authors would also like to thank Professor D.W. Shoesmith for his encouragement and helpful discussion throughout this project.

References

[1] V. Malinovschi, C. Ducu, N. Aldea, M. Fulger, J. Nucl. Mater. 352 (2006) 107.
[2] X. Zhang, W. Xu, D.W. Shoesmith, J.C. Wren, Corros. Sci., in press. Available online 26 July 2007.
[3] H. Antony, S. Peulon, L. Legrand, A. Chaussé, Electrochim. Acta 50 (2004) 1015.
[4] T.P. Niesen, M.R. De Guire, J. Electroceram. 6 (2001) 169.
[5] C.D. Lokhande, Mater. Chem. Phys. 27 (1991) 1.
[6] I. Grozdanov, Semicond. Sci. Technol. 9 (1994) 1234.
[7] P.K. Nair, M.T.S. Nair, V.M. Garcia, O.L. Arenas, Y. Peña, A. Castillo, I.T. Ayala, O. Gomezdaza, A. Sánchez, J. Campos, H. Hu, R. Suárez, M.E. Rincón, Sol. Energy Mater. Sol. Cells 52 (1998) 313.
[8] O. Savadogo, Sol. Energy Mater. Sol. Cells 52 (1998) 361.
[9] R.S. Mane, C.D. Lokhande, Mater. Chem. Phys. 65 (2000) 1.
[10] H. Nagayama, H. Honda, H. Kawahara, J. Electrochem. Soc. 135 (1998) 2013.
[11] A. Hishinuma, T. Goda, M. Kitaoka, S. Hayashi, H. Kawahara, Appl. Surf. Sci. 48&49 (1991) 405.
[12] S. Deki, Y. Aoi, J. Okibe, H. Yanagimoto, A. Kajinami, M. Mizuhata, J. Mater. Chem. 7 (1997) 1769.
[13] W. Mindt, J. Electrochem. Soc. 117 (1970) 615.
[14] W. Mindt, J. Electrochem. Soc. 118 (1971) 93.
[15] D. Raviendra, J.K. Sharma, J. Phys. Chem. Solids 46 (1985) 945.
[16] E. Matijevic, Ann. Rev. Mater. Sci. 15 (1985) 483.
[17] T.M. Devine, Corros. Sci. 37 (1995) 17.
[18] C.M. Flynn, Chem. Rev. 84 (1984) 31.
[19] P.C. Rieke, B.D. Marsh, L.L. Wood, B.J. Tarasevich, J. Liu, L. Song, G.E. Fryxell, Langmuir 11 (1995) 318.
[20] U. Schwertmann, R.M. Cornell, Iron Oxide in the Laboratory, 2nd Ed., Wiley, New York, 2000, p. 93.